A Machine Learning Approach on SMOS Thin Sea Ice Thickness Retrieval

Ferran Hernández-Macià, Carolina Gabarró, Gemma Sanjuan Gomez, and Maria José Escorihuela

***Abstract*—This study proposes a machine learning based methodology for estimating Arctic thin sea ice thickness (up to 1 m) from brightness temperature measurements of SMOS. The approach involves employing the so-called Burke model for sea ice emission modeling, integrating a suitable permittivity model and a radiative transfer equation. The training dataset is generated through a model-based simulation, and is then used to train and evaluate two machine learning regression algorithms: Random Forest and Gradient Boosting. Overall, this machine learning methodology results in great agreement with the ESA's official sea ice thickness product. Additionally, a validation performed by using data from mooring measurements shows a subtle improvement by the machine learning algorithms with respect to the ESA's official product. These results indicate their potential to surpass the performance of the current SMOS thin sea ice thickness retrievals.**

***Index Terms*—Gradient Boosting (GB), machine learning, random forest (RF), sea ice thickness, soil moisture and ocean salinity (SMOS) satellite.**

I. Introduction

SEA ice is an essential component of the Arctic's physical environment and serves as a crucial indicator of climate change. It has a key role in the ice-albedo feedback loop, as it acts as a reflective surface that helps to regulate the planet's temperature by reflecting sunlight back into space, reducing the amount of solar energy that is absorbed by the Earth's surface ([1]). Sea ice extension and thickness have been decreasing rapidly from the last decades on ([2]). As highlighted in the latest *Special Report on the Ocean and Cryosphere in a Changing Climate*, a component of the IPCC 2019 report ([3]), the Arctic sea ice extent is experiencing a rapid decline, amounting to approximately 13% per decade in September. This negative trend has also led to a notable transition to younger and thinner ice, with a decline of 30% to 2% in the proportion of ice at least five years old since 1979. Concurrently, there has been an increase in first-year ice, ranging from 40% to $60-70\%$ over the same period.

Radar altimeters have been utilized since the 1990's decade with the launch of the European Remote Sensing satellites 1 and 2 to generate Arctic sea ice thickness maps (ERS-1, 1991–2000, and ERS-2, 1995–2011). These first missions presented a too large footprint ([4]), later improved with their successor Envisat (2002–2012). Following the launch of CryoSat-2 (2010–present) and ICESat-2 (2018–present) altimeters, major advances have been made in the sea ice thickness retrievals accuracy ([5], [6]). Nowadays, by measuring the sea ice freeboard, the total sea ice thickness can be computed for sea ice thicker than 1 m ([7]). Passive microwave radiometers have been used to observe sea ice since the launch of the first Earth Observation satellites in the 1970's, and are still in use today with the European Space Agency (ESA) mission Soil Moisture and Ocean Salinity (SMOS) ([8], [9]) spacecraft launched on 2009, along with the National Aeronautics and Space Administration (NASA) missions: the past Advanced Microwave Scanning Radiometers (AMSR, AMSR-E, AMSR-2), and the Soil Moisture Active Passive (SMAP) ([10]) satellite which was launched on 2015. Specifically, this study focuses on passive L-band radiometers like SMOS, which operate at a frequency of 1.4 GHz and have a penetration depth of up to 1 m or even more in low salinity sea ice, thus being complementary to measurements with altimeters ([11]).

There exist two SMOS sea ice thickness algorithms for the non-melting period, i.e. from October to April. The first is the ESA's official product, which is a semi-empirical algorithm developed by the Alfred Wegener Institute (AWI), described in [12]. A notable drawback is its failure to account for the presence of snow above sea ice, which is a major limitation given its relevant effect on emitted L-band radiation ([13]) and subsequent thickness retrieval processes. The second product is distributed by the University of Bremen (UB), it is described in [14] and it uses an empirical approach. The primary shortcoming of the UB product lies in its limited sensitivity, extending only up to 0.5 m. This study attempts to advance towards the development of a new SMOS sea ice thickness product using an artificial intelligence approach. Previous works have successfully applied machine learning in sea ice remote sensing. For instance, in [15], sea ice thickness is derived from the FSSCat ([16]) nanosatellite data using a neural network approach. Other neural network

Manuscript received 4 January 2024; revised 22 April 2024 and 17 May 2024; accepted 21 May 2024. Date of publication 31 May 2024; date of current version 14 June 2024. This work was supported by the AEI with the ARCTIC-MON Project(PID2021-125324OB-I00) and also with the Programación Conjunta Internacional project called "MEJORANDO LOS MODELOS DE EMISIVIDAD DEL HIELO MARINO EN LAS MICROONDAS DE BAJA FRECUENCIA" (ICE-MOD), with reference PCI2019-111844-2. This work is also supported by the Spanish government through the "Severo Ochoa Centre of Excellence" accreditation (CEX2019-000928-S). *(Corresponding author: Ferran Hernández-Macià.)*

Ferran Hernández-Macià is with the Institute of Marine Sciences (ICM-CSIC), 08003 Barcelona, Spain, and also with the isardSAT S.L., 08005 Barcelona, Spain (e-mail: fhernandezmacia@icm.csic.es).

Carolina Gabarró is with the Institute of Marine Sciences (ICM-CSIC), 08003 Barcelona, Spain.

Gemma Sanjuan Gomez is with the Autonomous University of Barcelona (UAB), 08193 Cerdanyola del Vallès, Spain.

Maria José Escorihuela is with the isardSAT S.L., 08005 Barcelona, Spain.

Digital Object Identifier 10.1109/JSTARS.2024.3406921

based approach examples can be found in [17] and [18]. The method proposed in this work inherently takes into account the presence of snow above sea ice, while also preserving its sensitivity up to a depth of 1 m. The machine learning (ML) methodology will be trained using a sea ice microwave emission model, given the absence of in situ data. The input features for this approach include the brightness temperature (TB) itself, as well as the parameters influencing it at L-band frequency, the sea ice temperature, salinity, and the presence of snow. The targeted output variable is the thin sea ice thickness.

The article is structured as follows. Section II introduces sea ice microwave emission modeling, presenting the Burke model and discussing permittivity modeling. Section III provides an overview of the data collection utilized in this study. Section IV outlines the workflow followed in the proposed methodology. Section V presents the results, including an evaluation against an existing product and a validation using in situ data. Section VI contains a discussion of the results obtained with the proposed approach. Finally, Section VII offers the conclusions.

II. Sea Ice Microwave Emission Modeling

The Burke model can be used to simulate the emission of sea ice layered mediums in polar regions ([19]). This model considers factors such as thickness, temperature, salinity, and dielectric constant of the different layers to calculate the emissivity, so the brightness temperature can be then computed at a given frequency.

A. Burke Model: Radiation Transfer Equation

The Burke model, which is based on a radiation transfer model for soil microwave emissivity presented in [20], is chosen in this work to simulate the Arctic sea ice emission. The model makes certain assumptions, including that the radiation is treated with the conservation of energy approach (i.e. incoherent), that there is no emission or attenuation between the surface and the sensor, and that the sky has an isotropic brightness temperature of 5 K. Additionally, the model assumes that the layers are homogeneous, with constant permittivity, temperature, and salinity throughout each layer, and that the surface is smooth. Integrating for all the layers, the detected brightness temperature is a combination of the radiation emitted by the layered medium and the radiation reflected by the sky. The original derivation of the radiation transfer equation can be found in [20].

As this model considers media as layered, four layers are considered in this work: air–snow–ice–water, with the first and the last considered to be semi-infinite. The sea ice temperature and salinity values determine the permittivity, and are also used as input parameters. The snow layer is assumed to be isothermal with the underlying ice layer, non-saline, and it has a thickness equivalent to 10% of the ice thickness, as suggested in [21]. As shown by [13], the relative impact of the snow amount can be neglected, as the brightness temperature measured by the satellite at L-band is not influenced by the amount of snow above the ice, only by its presence. Lastly, the seawater is treated as a semi-infinite layer and is assumed to have typical Arctic values, with a temperature of -1.8$^\circ C$ and a salinity of 33.

B. Complex Dielectric Constant Modeling

The dielectric constant of the media is a key parameter for the sea ice emission modeling. It can be represented in a complex formulation: the permittivity constitutes the real part, while the imaginary part is the loss, which is directly proportional to the electrical conductivity. Higher permittivity indicates less penetration, whereas higher loss denotes more energy dissipation. Hereafter, the terms "dielectric constant" and "permittivity" are used interchangeably, as usually done in the bibliography. In [22], an empirical linear relationship between the brine volume fraction and the complex dielectric constant is established, which is valid for both first-year and multi-year sea ice. Interpolating the fit parameters at the L-band frequency, i.e. 1.4 GHz, from [22]:

$$\epsilon' = 3.1 + 0.0084 V_b \times 10^3, \tag{1}$$

$$\epsilon'' = 0.037 + 0.00445 V_b \times 10^3, \tag{2}$$

where V_b is the brine volume fraction. This parameter is obtained from the [23] coefficients for $T_{ice} \geq -2\,^\circ C$, and from the [24] coefficients for $T_{ice} < -2\,^\circ C$. In any case, this volume of brine is computed as ([22]):

$$V_b = \frac{\rho_i S_{ice}}{F_1 - \rho_i S_{ice} F_2}, \tag{3}$$

where $\rho_i = 0.917 - 0.1404 \times 10^{-3} T_{ice}$ is the pure ice density in gm^{-3} obtained from [25], and T_{ice} and S_{ice} are the temperature and salinity of the sea ice, respectively. F_1 and F_2 are T_{ice}'s polynomial functions of third degree, for which its constant coefficients can be found in [24].

Finally, it is remarkable that the real part of the complex dielectric constant for the snow layer is obtained from [26], while the imaginary part is extracted from [27] and [28]. This formulation is dependent on the snow density, and a typical value for the Arctic of $0.3 gcm^{-2}$ is used ([29]). Also, the complex permittivity of seawater is obtained from [30], in which a standard Arctic Ocean salinity of 33 is assumed.

III. Data Collection and Management

A. ESA Official SMOS Sea Ice Thickness Product

The *SMOS L3 Sea Ice Thickness* product is produced by the AWI and distributed by the ESA, and it provides information on sea ice thickness in the Arctic region from October to April, covering the period from 2010 to the present. It was firstly described in [12]. The sea ice thickness is determined using an iterative retrieval algorithm that incorporates a thermodynamic sea ice model and a three-layer radiative transfer model. The radiative transfer model calculates the emissivity of the sea ice layer and the underlying seawater, and brightness temperatures are derived from the emissivity and physical temperatures of the sea ice and seawater. The bulk ice temperature is estimated using a thermodynamic model, which utilizes the 2 m air temperature from atmospheric reanalysis data as an input parameter, while the bulk ice salinity is computed from an empirical relation described in [31]. The retrieval algorithm also accounts for variations in ice thickness within the SMOS spatial resolution by

using a statistical thickness distribution function based on high-resolution ice thickness measurements from NASA's Operation IceBridge (OIB) campaign.

In this work, the TB intensity measured by SMOS is obtained from this ESA official SMOS sea ice thickness product, to be then used as input of the methodology.

B. Surface Temperature Satellite Product

The *Arctic Ocean - Sea and Ice Surface Temperature REPROCESSED* product ([32]) provides information on the Arctic sea and ice surface temperature. The data is based on reprocessed observations from the Advanced Very High Resolution Radiometer (AVHRR), the Advanced Along Track Scanning Radiometers (AATSR), and the Sea and Land Surface Temperature Radiometer (SLSTR), which are obtained from various sources, including the ESA Climate Change Initiative (CCI) project, the Copernicus Climate Change Service (C3S) project, and the Arctic & Antarctic Ice Surface Temperatures from Thermal Infrared Satellite Sensors (AASTI) dataset. The product offers a daily interpolated field with a 0.05 degrees resolution and covers surface temperatures in the ocean, the sea ice, and the marginal ice zone. The computation of the surface temperature utilizes the optimal interpolation method, utilizing the previous day value as a first guess field.

In this work, a linear temperature gradient within the ice is assumed, as it is shown to be reasonably realistic in [33]. Therefore, the bulk ice temperature (T_{ice}) can be computed as:

$$T_{ice} = \frac{T_{surface} - T_{sw}}{2}, \tag{4}$$

where $T_{surface}$ is the surface temperature obtained from the satellite product, and T_{sw} is the seawater temperature, in which a typical value for the Arctic of $-1.8°C$ is assumed.

C. Arctic Ocean Physics Reanalysis Model

The *Arctic Ocean Physics Reanalysis* model product distributed by CMEMS ([34]) provides physical variables obtained from the reanalysis model TOPAZ (version 4b). It assimilates a variety of observations, such as sea level anomalies from satellite altimeters, sea surface temperature from Operational Sea Surface Temperature and Sea Ice Analysis (OSTIA), in situ temperature and salinity from hydrographic cruises and moorings, sea ice concentration from OSI-SAF, the CS2SMOS ice thickness data, and sea surface salinity from the Barcelona Expert Center (BEC) using SMOS satellite data. For the purpose of this work, the seawater salinity, the sea ice thickness and the snow depth variables are extracted from this model. To obtain the bulk ice salinity, the empirical formula from [31] is used:

$$S_{ice} = S_{sw}(1 - S_R)e^{-a\sqrt{d_{ice}}} + S_R S_{sw}, \tag{5}$$

where S_{sw} is the seawater salinity and d_{ice} the sea ice thickness in cm, both obtained from the reanalysis model. The growth rate coefficient, denoted as a, is assumed to be 0.5, while for S_R, the salinity ratio of the bulk ice salinity at the end of the ice growth season, 0.175 is taken. Finally, the snow presence is simply taken as a boolean variable: if the snow thickness variable from TOPAZ is greater than 0, then snow is present, and otherwise it is absent.

D. BGEP Mooring Data

The Beaufort Gyre Exploration Project (BGEP) ULS are mooring buoys designed to measure the sea ice draft, which is the part of sea ice that remains underwater. Therefore, to obtain the total sea ice thickness, which is the required variable to validate the proposed methodology, a conversion is needed. As done in [35], a factor of 1.136 is used to multiply the ice draft and thus obtain the total thickness. This coefficient was obtained empirically from almost 400 sea ice drillings conducted in Fram Strait ([36]). The BGEP ULS data is used for the methodology validation. It comprises daily averages of sea ice thickness from three mooring instruments located within the Beaufort Gyre. The sampling periods cover years between 2003 and 2021. However, only the data gathered since the launch of SMOS in 2010 is suitable to be used in this study.

IV. Methodology

The in situ data available for the Arctic region is very sparse. Since no complete thin sea ice thickness dataset is available, it can be generated through sea ice emission modeling. This methodology's workflow is summarized in Fig. 1. Prior to this, all the variables are regridded to the 12.5 km x 12.5 km NSIDC Polar Stereographic grid. As shown, for testing, and also for validation and predicting in general, the same variable sources are used, with the difference of the modeled sea ice thickness being only used during training as it is the target variable, which is predicted. The training dataset is thus composed of the cells extracted from the map of each day, after dropping the duplicates, from 15th October 2019 to 15th April 2020 and from 15th October 2020 to 15th April 2021. The testing is performed during January 2022. Finally, the validation is done with the BGEP mooring data of the sea ice growth period of each year from 2010 to 2020.

The Burke emission model assuming the Vant formulation for the ice permittivity is inverted to obtain realistic configurations of Arctic sea ice thickness distributions, with the aim of generating a reproducing situations as realistic as possible. This is detailed in Fig. 2. As it is shown, the different variables detailed in Section III are regridded to the same grid, as they are then used to invert the physical emission model to compute the sea ice thickness. It should be noted that the primary variables extracted from the different sources are transformed as it is detailed in Section III and in Fig. 1: the sea ice temperature is computed from the surface temperature by assuming a linear gradient within the ice, and the sea ice salinity is obtained through an empirical equation ([31]) that has the sea water salinity and the reanalysis sea ice thickness as inputs.

The sensitivity of the brightness temperature to the ice thickness at this frequency band is highly dependent on the ice conditions, i.e. temperature and salinity, as shown in Fig. 3. To avoid an artificial training threshold, for each ice conditions configuration the maximum thickness that can be retrieved (the value where the brightness temperature starts to saturate) is

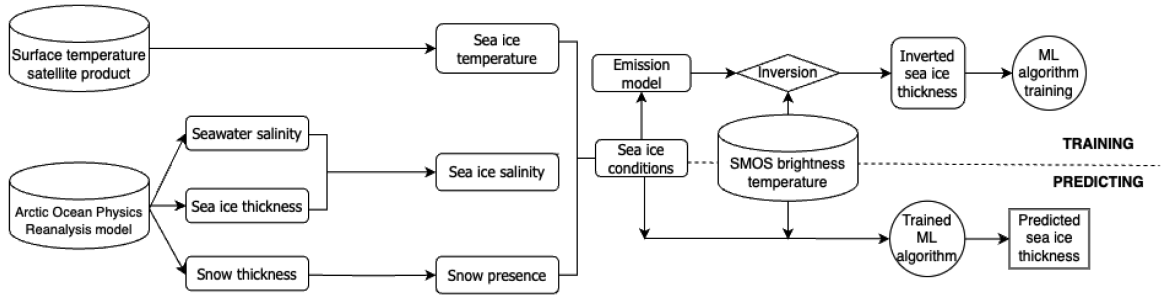

Fig. 1. Diagram of the methodology's workflow. The variable extracted from different sources are input to an emission model to simulate the sea ice thickness distribution. After training the algorithm, the same variables, except the modeled sea ice thickness as it is the target variable, are used to perform predictions.

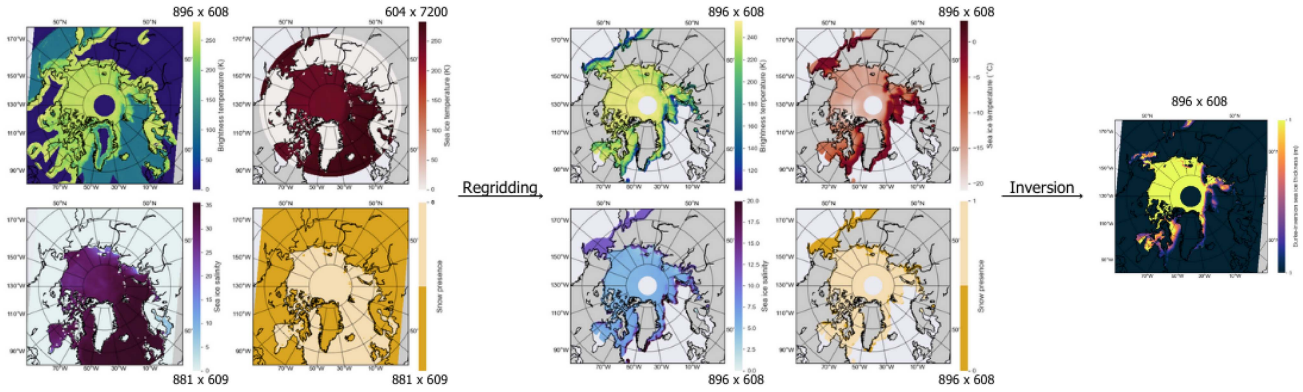

Fig. 2. Regridding the brightness temperature, the surface temperature, the sea water salinity (and the reanalysis sea ice thickness even though it is now shown), and the snow presence to the same common grid (12.5 km x 12.5 km NSIDC Polar Stereographic). These transformed variables are then used to invert the Burke emission model to obtain the sea ice thickness for the training dataset.

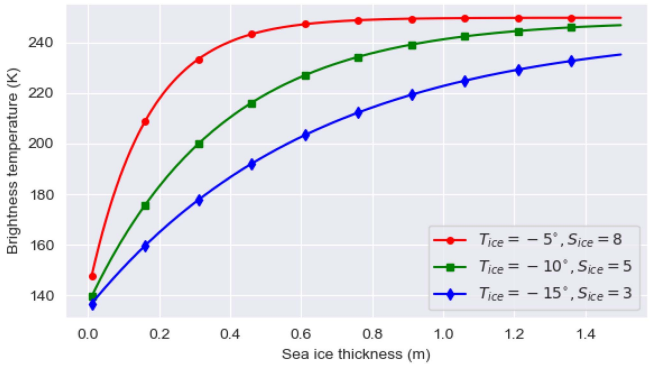

Fig. 3. Brightness temperature as a function of the sea ice thickness for different combinations of sea ice conditions, computed with the Burke model.

computed. Subsequently, the thickness obtained from the model inversion is compared to the maximum thickness: if the latter is smaller, the inverted solution is then this maximum thickness.

Single data cells from these complete maps are extracted and input to train the algorithm. Therefore, the modeled sea ice thickness obtained through model inversion, along with the sea ice temperature from the sea ice surface temperature satellite product, and the sea ice salinity and the snow presence derived from the reanalysis model, are used to train the ML algorithm. Regarding the snow presence, even though it increases the ice temperature by acting as an insulator, it is only the snow–ice interface that affects the emitted radiation. Therefore, the algorithm is trained for the only two possible significantly different situations, i.e. sea ice free of snow, and sea ice with any amount of snow above it.

Focusing on supervised learning, in particular on regression methods, the machine learning algorithms selected for this purpose are the Random Forest (RF, [37]) and the Gradient Boosting (GB, [38]). Random Forest for regression builds an ensemble of decision trees. Each tree is trained on a random subset of data and features. During prediction, individual tree outputs are averaged to get the final result. This technique, called bagging, reduces overfitting and improves generalization. Gradient Boosting builds also an ensemble of decision trees sequentially, where each tree corrects errors made by the previous one. During training, each new tree focuses on the residuals (the differences between the actual and predicted values) of the ensemble so far. Their learning process involves adjusting the parameters of each tree to reduce the residuals, and the final prediction is the sum of predictions from all trees.

Therefore, both algorithms are more powerful generalizations of the decision trees, and although they have many similarities, they differ in how the trees are build and combined. Both have common advantages for which seem reasonable to be

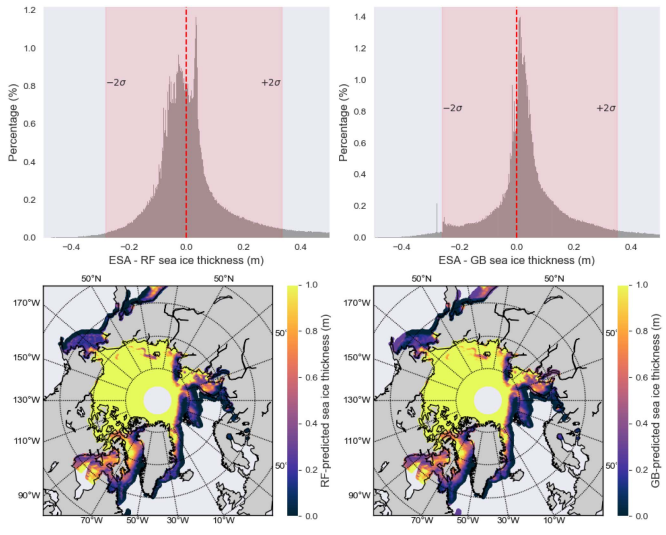

Fig. 4. **(a)** Upper: Histograms of the difference between the ESA's official sea ice thickness product and the predicted sea ice thickness using the Random Forest and the Gradient Boosting algorithms, respectively, for January 2022. **(b)** Lower: Arctic sea ice thickness maps generated with the Random Forest and Gradient Boosting algorithms, respectively, for 31st January 2022.

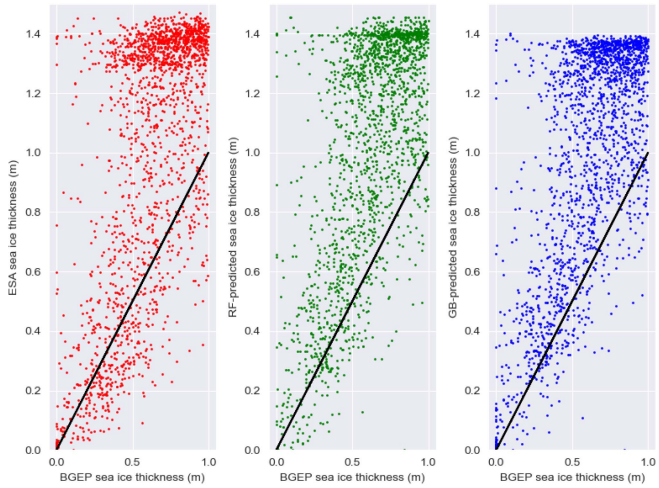

Fig. 5. Scatter plots of the ESA official product and the machine learning algorithms, the RF and the GB, as a function of the BGEP moorings in situ data.

TABLE I
R^2 CORRELATION COEFFICIENT, MEAN ABSOLUTE ERROR (MAE) AND STANDARD DEVIATION OF THE MEAN ABSOLUTE ERROR (STD-MAE) OF THE VALIDATION USING BGEP MOORING DATA

Metric	ESA	RF	GB
R^2	0.673	0.714	0.706
MAE (m)	0.424	0.405	0.389
std-MAE (m)	0.287	0.271	0.262

selected for this work, such as that they generally require less data cleaning and preprocessing compared to neural networks. They are also little influenced by outliers, and they present good scalability, being applicable to datasets with numerous observations. Furthermore, the computation resources required by these algorithms are considerably lower than in a neural network approach. A drawback of these RF and GB algorithms is that the interpretability compared to models based on a single tree is reduced, because in this case multiple trees are combined. Both algorithms are directly implemented from the Python's library *scikit-learn* (https://scikit-learn.org). Specifically, they are used with 50 estimators, as it is found as a reasonable number after trying other options ranging from 10 to 1000. No more hyperparameters are tuned after testing without improving the results.

V. RESULTS

To test the methodology, the predictions performed as shown in Fig. 1 are compared with ESA's official sea ice thickness product in a suitable period which does not correspond to the training period: January 2022. Fig. 4(a) shows the differences between the ESA's official sea ice thickness product and the values predicted using the RF and GB algorithms for each day of January 2022. The distribution is similar for both algorithms, with the major number of differences being around zero. Therefore, the machine learning approach presents a similar distribution compared to the ESA's product. An equivalent number of values are under and overestimated by the RF and the GB, although the RF has a more symmetric distribution while the GB presents more predictions with no difference with ESA's. Remarkably, both algorithms have similar 2σ ranges, thus resulting in equivalent differences. Overall, the metrics computed from this comparison result in a correlation coefficient of 0.956 for the RF and of 0.955 for the GB, and a mean absolute error of 0.099 m for the RF and of 0.104 m for the GB. Fig. 4(b) shows 31st January 2022 as an example, and it depicts this similarity between the RF and GB, presenting alike maps.

Despite the satisfactory results obtained after the comparison with the ESA's official product, it cannot be fully concluding as the ESA product also relies on a semi-empirical model. For this reason, a source of ground truth data is required to further validate the methodology. The mooring data from the BGEP ULS is used for this purpose. The ESA, RF, and GB sea ice thickness' are interpolated to the exact position of each mooring for each day during the periodical measurements from 2010 to 2021. Fig. 5 shows the scatter plots of the ESA, RF, and GB predictions interpolated to the mooring coordinates as a function of the BGEP moorings data. It is remarkable that only the points below 1 m are considered in the analysis.Although the metrics are reasonable for the three algorithms as shown in Table I, the ML algorithms present a higher correlation and a lower error than the ESA product when comparing to the in situ data, as well as less biased predictions as depicted by the std-MAE. Furthermore, they all present many values around 1.4 m. These points are identified to be mainly the same for the ESA product and the ML methodology. It can be hypothesized that it is because when the ice reaches this thickness', given the temperature and salinity conditions, the saturation region shown in Fig. 3 is reached.

VI. Discussion

The results presented in Section V suggest that the proposed methodology has the potential to improve the current SMOS thin sea ice thickness retrievals. Even thought great results have been obtained, some aspects can be discussed to assess the robustness of the methodology. An important observation is that, even though these ML algorithms are trained to predict the sea ice thickness point by point, the maps from Fig. 4 show a continuous and smooth distribution around the whole Arctic. Fig. 2 shows the different input variables for 31st January 2022, after the rocessing depicted in Section IV, presenting also continuous and spatially-coherent distributions. The nearby similar conditions from these inputs help in predicting robust thickness maps. This highlights the power of this methodology to generalize, as solid and coherent maps are predicted for any period of time after training with only two seasons (2019–2020 and 2020–2021).

Another key for the possible success of this methodology is its simplicity and the limited amount of computational resources that it needs. As stated in Section IV, the RF and GB algorithms require much less resources than neural network approaches, or even classical algorithms. Furthermore, no in situ data is needed to feed these algorithms, given the promising results obtained in the in situ validation. However, it is important to mention that new in situ measurements may improve the sea ice emission modeling that thus would increase the quality of the retrieval. Ultimately, despite the evident spatial coherence in the predicted maps, there remains an opportunity to explore more advanced deep learning algorithms to incorporate not only spatial but also temporal consistency. Therefore, this is left as future work to improve the current version of the algorithm.

VII. Conclusion

A machine learning based methodology to retrieve Arctic thin sea ice thickness from SMOS brightness temperature measurements has been successfully developed. Two different algorithms, a Random Forest and a Gradient Boosting, have been trained by extracting realistic data points from maps generated through inverting a sea ice L-band emission model. The evaluation of such algorithms by comparison with the current ESA official sea ice thickness has shown their high correlation and an almost negligible averaged absolute error. This indicates that this methodology is able to reproduce the predictions from the classic approach, reducing the complexity and the computational resources. The validation using the moorings' data as ground truth indicate a slight improvement by the ML algorithms. Finally, remains challenging to choose between the RF and the GB as they present similar results in the conducted analysis. These work shows the potential of the machine learning techniques to improve the current SMOS thin sea ice thickness retrievals.

Acknowledgment

The production of SMOS sea ice thickness data was funded by the ESA project SMOS & CryoSat-2 Sea Ice Data Product Processing and Dissemination Service, and data from 2010/10/15 to 2021/04/15 were obtained from AWI. The data were collected and made available by the Beaufort Gyre Exploration Program based at the Woods Hole Oceanographic Institution (https://www2.whoi.edu/site/beaufortgyre/) in collaboration with researchers from Fisheries and Oceans Canada at the Institute of Ocean Sciences.

References

[1] M. I. Budyko, "The effect of solar radiation variations on the climate of the Earth," *Tellus*, vol. 21, no. 5, pp. 611–619, 1969. [Online]. Available: https://onlinelibrary.wiley.com/doi/abs/10.1111/j.2153-3490.1969.tb00466.x

[2] R. Kwok, "Arctic sea ice thickness, volume, and multiyear ice coverage: Losses and coupled variability (1958–2018)," *Environ. Res. Lett.*, vol. 13, no. 10, Oct. 2018, Art. no. 105005, doi: 10.1088/1748-9326/aae3ec.

[3] M. Meredith et al., "Polar regions," in *IPCC Special Report on the Ocean and Cryosphere in a Changing Climate*. Cambridge, U.K.: Cambridge Univ. Press, 2019, pp. 203–320.

[4] M. Bocquet et al., "Arctic sea ice radar freeboard retrieval from the European remote-sensing satellite (ers-2) using altimetry: Toward sea ice thickness observation from (1995 to 2021)," *Cryosphere*, vol. 17, no. 7, pp. 3013–3039, 2023. [Online]. Available: https://tc.copernicus.org/articles/17/3013/2023/

[5] S. W. Laxon et al., "CryoSat-2 estimates of arctic sea ice thickness and volume," *Geophysical Res. Lett.*, vol. 40, no. 4, pp. 732–737, 2013. [Online]. Available: https://agupubs.onlinelibrary.wiley.com/doi/abs/10.1002/grl.50193

[6] N. T. Kurtz, N. Galin, and M. Studinger, "An improved CryoSat-2 sea ice freeboard retrieval algorithm through the use of waveform fitting," *Cryosphere*, vol. 8, no. 4, pp. 1217–1237, 2014. [Online]. Available: https://tc.copernicus.org/articles/8/1217/2014/

[7] J. C. Landy et al., "A year-round satellite sea-ice thickness record from cryosat-2," *Nature*, vol. 609, no. 10, pp. 517–522, 2022.

[8] S. Mecklenburg, N. Wright, C. Bouzina, and S. Delwart, "Getting down to business - SMOS operations and products," *ESA Bull.*, vol. 137, pp. 25–30, 2009.

[9] Y. H. Kerr et al., "The SMOS mission: New tool for monitoring key elements of the global water cycle," *Proc. IEEE*, vol. 98, no. 5, pp. 666–687, May 2010.

[10] D. Entekhabi et al., "The soil moisture active passive (SMAP) mission," *Proc. IEEE*, vol. 98, no. 5, pp. 704–716, May 2010.

[11] R. Ricker, S. Hendricks, L. Kaleschke, X. Tian-Kunze, J. King, and C. Haas, "A weekly arctic sea-ice thickness data record from merged CryoSat-2 and SMOS satellite data," *Cryosphere*, vol. 11, no. 4, pp. 1607–1623, 2017. [Online]. Available: https://tc.copernicus.org/articles/11/1607/2017/

[12] X. Tian-Kunze et al., "SMOS-derived thin sea ice thickness: Algorithm baseline, product specifications and initial verification," *Cryosphere*, vol. 8, no. 3, pp. 997–1018, 2014. [Online]. Available: https://tc.copernicus.org/articles/8/997/2014/

[13] N. Maass, L. Kaleschke, X. Tian-Kunze, and R. T. Tonboe, "Snow thickness retrieval from L-band brightness temperatures: A model comparison," *Ann. Glaciol.*, vol. 56, no. 69, pp. 9–17, 2015.

[14] M. Huntemann, G. Heygster, L. Kaleschke, T. Krumpen, M. Mäkynen, and M. Drusch, "Empirical sea ice thickness retrieval during the freeze-up period from SMOS high incident angle observations," *Cryosphere*, vol. 8, no. 2, pp. 439–451, 2014. [Online]. Available: https://tc.copernicus.org/articles/8/439/2014/

[15] C. Herbert, J. F. Munoz-Martin, D. Llaveria, M. Pablos, and A. Camps, "Sea ice thickness estimation based on regression neural networks using L-band microwave radiometry data from the FSSCat mission," *Remote Sens.*, vol. 13, no. 7, 2021, Art. no. 1366. [Online]. Available: https://www.mdpi.com/2072-4292/13/7/1366

[16] A. Camps et al., "Fsscat, the 2017 copernicus master's "Esa sentinel small satellite challenge" winner: A federated polar and soil moisture tandem mission based on 6U cubesats," in *Proc. IEEE Int. Geosci. Remote Sens. Symp.*, 2018, pp. 8285–8287.

[17] Q. Yan, W. Huang, and C. Moloney, "Neural networks based sea ice detection and concentration retrieval from GNSS-R delay-doppler maps," *IEEE J. Sel. Topics Appl. Earth Observ. Remote Sens.*, vol. 10, no. 8, pp. 3789–3798, Aug. 2017.

[18] Q. Yan and W. Huang, "Sea ice sensing from GNSS-R data using convolutional neural networks," *IEEE Geosci. Remote Sens. Lett.*, vol. 15, no. 10, pp. 1510–1514, Oct. 2018.
[19] C. Gabarro, A. Turiel, P. Elosegui, J. A. Pla-Resina, and M. Portabella, "New methodology to estimate arctic sea ice concentration from smos combining brightness temperature differences in a maximum-likelihood estimator," *Cryosphere*, vol. 11, no. 4, pp. 1987–20022017. [Online]. Available: https://tc.copernicus.org/articles/11/1987/2017/
[20] W. Burke, T. Schmugge, and J. Paris, "Comparison of 2.8- and 21-cm microwave radiometer observations over soils with emission model calculations," *J. Geophysical Res.*, vol. 84, pp. 287–294, 1979.
[21] Y. Doronin, *Thermal Interaction of the Atmosphere and the Hydrosphere in the Arctic*. Philadelphia, PA, USA: CoronetBooks, 1971.
[22] M. Vant, R. Ramseier, and V. Makios, "The complex-dielectric constant of sea ice at frequencies in the range 0.1–40 GHz," *J. Appl. Phys.*, vol. 49, pp. 1264–1280, 1978.
[23] M. Leppäranta and T. Manninen, "The brine and gas contents of sea-ice with attention to low salinities and high temperatures, internal report 2," Finnish Institute of Marine Research, Tech. Rep., 1998.
[24] G. Cox and W. Weeks, "Equations for determining the gas and brine volumes in sea-ice samples," *J. Glaciol.*, vol. 29, no. 102, pp. 306–316, 1983.
[25] E. Pounder, "The physics of ice. Oxford, Pergamon Press. (The commonwealth and international library, geophysics division)," *J. Glaciology*, vol. 6, no. 44, 1965, Art. no. 315.
[26] C. Matzler, "Microwave permittivity of dry snow," *IEEE Trans. Geosci. Remote Sens.*, vol. 34, no. 2, pp. 573–581, Mar. 1996.
[27] M. Tiuri, A. Sihvola, E. Nyfors, and M. Hallikaiken, "The complex dielectric constant of snow at microwave frequencies," *IEEE J. Ocean. Eng.*, vol. 9, no. 5, pp. 377–382, Dec. 1984.
[28] C. Mätzler, *Thermal Microwave Radiation: Applications for Remote Sensing*. Piscataway, NJ, USA: Inst. Elect. Engineers, 2006.
[29] S. G. Warren et al., "Snow depth on arctic sea ice," *J. Climate*, vol. 12, no. 6, pp. 1814–1829, Jun. 1999.
[30] L. Klein and C. Swift, "An improved model for the dielectric constant of sea water at microwave frequencies," *IEEE Trans. Antennas Propag.*, vol. 2, no. 1, pp. 104–111, Jan. 1977.
[31] A. I. Ryvlin, "Method of forecasting flexural strength of an ice cover," *Probl. Arct. Antarct*, vol. 45, pp. 79–86, 1974.
[32] "Arctic ocean - sea and ice surface temperature REPROCESSED," [Online]. Available: https://data.marine.copernicus.eu/product/SEAICE_ARC_PHY_CLIMATE_L4_MY_011_016/description
[33] M. Huntemann, "Thickness retrieval and emissivity modeling of thin sea ice at L-band for SMOS satellite observations," Ph.D. dissertation, Staats- und Universitätsbibliothek Bremen, 2015.
[34] "Arctic ocean physics reanalysis," [Online]. Available: https://data.marine.copernicus.eu/product/ARCTIC_MULTIYEAR_PHY_002_003/description
[35] H. J. Belter et al., "Satellite-based sea ice thickness changes in the laptev sea from 2002 to 2017: Comparison to mooring observations," *Cryosphere*, vol. 14, no. 7, pp. 2189–2203, 2020. [Online]. Available: https://tc.copernicus.org/articles/14/2189/2020/
[36] T. Vinje and Ø. Finnekåsa, *The Ice Transport Through the Fram Strait* (ser. Norsk Polarinstitutt). Oslo: Skrifter, 1986.
[37] L. Breiman, "Random forests," *Mach. Learn.*, vol. 45, pp. 5–32, 2001.
[38] J. H. Friedman, "Stochastic gradient boosting," *Comput. Statist. Data Anal.*, vol. 38, no. 4, pp. 367–378, 2002, *Nonlinear Methods and Data Mining*.

Ferran Hernández-Macià received the bachelor's degree in physics from the Universitat de Barcelona, Barcelona, Spain, in 2022, and the master's degree in modeling for science and engineering, with specialization in complex systems modeling, in 2023 from the Universitat Autònoma de Barcelona (UAB), Bellaterra, Spain, where he is currently working toward the Ph.D. degree in collaboration with the Institut de Ciències del Mar (ICM-CSIC) and the company isardSAT, S.L, Barcelona.

His thesis is dedicated to the sea ice thickness retrievals from radiometry and altimetry observations, with special emphasis also on the physical modelling of sea ice and its impact on the retrieval algorithms. His research focuses on the usage of remote sensing to study the cryosphere.

Carolina Gabarró received the Engineering and Ph.D. degrees in physics from the Universitat Politècnica de Catalunya, Barcelona, Spain in 1998 and 2004, respectively.

From 1997 to 1999, she was with the European Space Agency (ESA), at ESTEC and ACRI. In 2000, she joined the Institute of Marine Sciences, ICM-CSIC, in Barcelona with the focused on the ESA's SMOS (Soil Moisture and Ocean Salinity) mission, developing and implementing algorithms to derive the sea surface salinity and sea ice thickness from the L-band microwave radiometer data. In 2007, she participated in the creation of the Barcelona Expert Center (BEC, bec.icm.csic.es), where she has been the Executive Director since 2012. She has led and participated in several national and international polar projects (Arctic+SSS from ESA, KEPLER, CriceS from H2020, AEI) and on the largest international Arctic expedition, MOSAiC. Since 2016, she has been the Spanish delegate in the Cryosphere group at the International Arctic Science Committee. She is currently the Head of the Cryosphere Group, BEC, and the Physical Oceanography and technology Department, ICM, Barcelona.

Gemma Sanjuan Gomez received the bachelor's degree in physics from Universitat Autònoma de Barcelona (UAB), Bellaterra, Spain, in 2011, the Mechanical Engineering degree from Universitat Politècnica de Catalunya (UPC), Barcelona, Spain, in 2011, dual master's degree in modeling for science and engineering in 2012 and in high performance computing, information theory, and security from UAB in 2012 and 2013, respectively.

In 2013, she joined the High Performance Computing Applications for Science and Engineering group at the Computer Architecture and Operating Systems Department, UAB. She did a Ph.D. thesis on acceleration of wind field models calculation by applying data and functional parallelism, advised by Prof. Tomàs Margalef. Her research interests include developing algorithms and Big Data.

Maria José Escorihuela received the Engineering degree in electronics and telecommunications from the Universitat Politècnica de Catalunya, Barcelona, Spain, in 1996, and the Ph.D. degree in environmental, space, and universe sciences from the "Institut National Polytechnique," Toulouse, France, in 2006.

In 2008, she joined isardSAT, S.L, Barcelona, Spain, where she is currently a Senior Research Scientist. She has 20 years of experience in microwave remote sensing. She has been actively involved in the development and validation of models and algorithms to retrieve geophysical variables from microwave satellite data. Her research interests include the application of remote sensing using passive and active microwave to the study of the biosphere and cryosphere in the areas of hydrology and climate change.